

Published in final edited form as:

Biochemistry. 2007 March 13; 46(10): 2787-2796. doi:10.1021/bi0616596.

# Water Structural Changes in the L and M Photocycle Intermediates of Bacteriorhodopsin as Revealed by Time-Resolved Step-Scan FTIR Spectroscopy

Joel E. Morgan<sup>1</sup>, Ahmet S. Vakkasoglu<sup>2</sup>, Robert B. Gennis<sup>2,3</sup>, and Akio Maeda<sup>3,\*</sup>
<sup>1</sup>Department of Biology, Center for Biotechnology and Interdisciplinary Studies, Room 2237, Rensselaer Polytechnic Institute, 110 Eighth St., Troy, NY 12180

<sup>2</sup>Center for Biophysics and Computational Biology, University of Illinois at Urbana/Champaign, Urbana, IL, 61801

<sup>3</sup>Department of Biochemistry, University of Illinois at Urbana/Champaign, Urbana, IL 61801

# **Abstract**

In previous FTIR studies of the photocycle intermediates of bacteriorhodopsin at cryogenic temperatures, water molecules were observed in the L intermediate, in the region surrounded by protein residues between the Schiff base and Asp96. In the M intermediate, the water molecules had moved away towards the Phe219-Thr46 region, but in the N intermediate they were again observed near the Schiff base. In order to evaluate the relevance of this scheme at room temperature, time resolved FTIR difference spectra of bacteriorhodopsin, including the water O-H stretching vibration frequency regions, were recorded in the usec and msec time ranges. Vibrational changes of weakly-H-bonded water molecules were observed in L. M. and N. In each of these intermediates, the depletion of a water O-H stretching vibration at 3645 cm<sup>-1</sup> originating from the initial unphotolzyed bacteriorhodopsin was observed as a trough in the difference spectrum. This vibration is due to the dangling O-H group of a water molecule which interacts with Asp85, and its absence in each of these intermediates indicates that there is perturbation of this O-H group. The formation of M is accompanied by the appearance of water O-H stretching vibrations at 3670 and 3657 cm<sup>-1</sup>. These bands are due to water molecules present in the region surrounded by Thr46, Asp96 and Phe219. Formation of L at 298 K is accompanied by the perturbations of Asp96 and the Schiff base, though in different ways from what is observed at 170 K. Changes in a broad water vibrational feature, centered around 3610 cm<sup>-1</sup>, are kinetically correlated with the L-to-M transition. These results imply that even at room temperature, water molecules interact with Asp96 and the Schiff base in L, though with a less rigid structure than at cryogenic temperatures.

Bacteriorhodopsin is a light-driven proton pump. It undergoes a photocycle initiated by the absorption of light by a retinal chromophore which is covalently linked to Lys216 forming a protonated Schiff base. The initial consequence of light absorption is the trans-to-cis isomerization of the  $C_{13}$ = $C_{14}$  bond of the retinal. Proton pumping takes place as the protein undergoes conformational changes from the initial unphotolyzed state with an all-trans retinal chromophore (BR  $^1$ ) through a sequence of intermediates, and back to the BR state. Spectroscopic and kinetic studies, including FTIR studies have distinguished a sequence of

<sup>&</sup>lt;sup>+</sup>This work was supported by an NIH grant HL 16101 (to RBG).

<sup>\*</sup>Author to whom correspondence should be addressed. Phone and Fax: +81-774-22-8781. akio.maeda@gmail.com.

<sup>&</sup>lt;sup>1</sup>Abbreviations. BR, the initial unphotolyzed state of bacteriorhodopsin with all-trans retinal chromophore; HOOP, hydrogen out-of-plane bending vibration; PRC, the proton release complex.

intermediates:  $BR \rightarrow K \rightarrow K_L \rightarrow L \rightarrow M_1 \rightarrow M_2 \rightarrow N \rightarrow O \rightarrow BR$  (1-4). These intermediates have different protonation states of Asp85, the Schiff base and Asp96. In the L intermediate, the initial state of the protein is maintained: unprotonated Asp85, protonated Schiff base and protonated Asp96. In the L-to-M transition the Schiff base deprotonates and Asp85 becomes protonated (5, 6). After a slight delay, a proton is released to the extracellular medium from the proton release complex (PRC) (7, 8). The M-to-N transition is accompanied by the reprotonation of the Schiff base and deprotonation of Asp96 (9, 10). During the N-to-O transition, the *cis*-to-*trans* re-isomerization of the  $C_{13}$ = $C_{14}$  bond (11) is accompanied by the uptake of a proton from the cytoplasmic medium to reprotonate Asp96 (12). Finally, the transfer of a proton from Asp85 to the PRC occurs as the O intermediate is converted back to the initial state (BR) (13).

Each proton transfer step must be induced by changes in the proton affinities of the residues involved. These changes in proton affinity are brought about by changes in the protein conformation, the orientation of the retinal Schiff base, and relocation of internal water molecules. These structural changes are, in turn, the result of the isomerization of the retinal chromophore. Changes in interaction with internal waters are expected to modulate the stability of the protonated and deprotonated states of protein residues, in particular Asp85, Asp96 and the Schiff base. Although there are remarkable crystallographic data revealing structural changes by means of trapped, static intermediate states (14-23), much remains unknown about the dynamics of the changes in molecular interactions that take place during the photocycle. FTIR spectroscopic studies have revealed changes in internal water molecules and key protein residues, Asp96 and the Schiff base, which occur during the photocycle. These changing interactions between internal water molecules and the protein play a major role in determining the pathways for proton transfers as well as the proton affinities of the groups within in the protein.

Studies performed at cryogenic temperatures on the water O-H stretching vibration bands in the 3750-3450 cm<sup>-1</sup> region in the L-minus-BR, M-minus-BR and N-minus-BR difference spectra have shown that internal water molecules undergo specific changes in location within the protein during the photocycle (see review 24). Water molecules stabilize the Lintermediate by filling a cavity surrounded by protein residues between the Schiff base and Asp96. In the M intermediate, these water molecules move to the Phe219-Thr46 region but return to the Schiff base region in N. An FTIR result shows that one of the O-H bonds of water molecules around Asp85 forms an H-bond in L (25) and in M (26). These studies suggested that internal water molecules play a critical functional role as a mobile structural element, filling cavities in specific conformations which may regulate proton affinity of the Schiff base, Asp85 and Asp96 in the light-driven proton pump. However, some of these interactions may be different at room temperature than at cryogenic temperatures where these observations were originally made. This possibility is suggested by the observation that the hydrogen out-of-plane bending vibration (HOOP) of the Schiff base in L at 170 K (27) is different from the ones detected in L at room temperature (28). Furthermore, the L intermediate produced by photoreaction at 170 K forms little or no M intermediate upon warming of the sample at least at neutral pH, and instead returns to the unphotolyzed BR state (29, 30).

The aim of the current work is to examine the changes in the O–H stretching vibrations of internal water molecules at room temperature in the µsec-to-msec time range of the photocycle. Until recently, time-resolved FTIR spectroscopic studies (9, 28, 31-34) focused on changes in the 1800-800 cm<sup>-1</sup> frequency region, which includes information about protein residues and the chromophore during the photocycle, but did not deal with the vibration bands of water molecules. Gerwert and his colleagues have successfully obtained time-resolved FTIR difference spectra at room temperature for two broad vibrational

features, one in the  $2200-1700~\rm cm^{-1}$  region (35, 36) and the other in the  $2900-2500~\rm cm^{-1}$  region (35, 37). The former has been assigned as a continuum band due to a proton delocalized in a H-bonding water network as proposed by Zundel (38) or to  $\rm H_5O_2^+$  (33, 36, 39, 40). Mutagenesis studies have shown that this protonated water network is located in the region between Glu204 and Glu194, and helps to form the PRC. The broad vibration bands in the  $2900-2500~\rm cm^{-1}$  region have been inferred to be due to strongly H-bonded water molecules from two different internal clusters, based largely on mutagenesis studies (35). There are also contributions in the initial state (BR) from a water cluster near the Schiff base that is disrupted in the early part of the photocycle (K and L), and from a second water cluster that develops strong H-bonds after the loss of the proton from the PRC (37). In *in situ*  $\rm H_2^{16}O/H_2^{18}O$  exchange experiments, Garczarek and Gerwert (37) also detected a water vibrational band at  $3642~\rm cm^{-1}$  in the initial state, which has been identified as arising from a water molecule that is hydrogen bonded to deprotonated Asp85 but whose second hydrogen has no interactions.

There is also the possibility that internal water molecules play a role in long range proton transfer from Asp96 to the Schiff base in the M-to-N transition (41). Such a water cluster between Asp96 and the Schiff base was detected by Schobert et al. (18) in the crystallographic structure of N of V49A, in which Asp96 is protonated (described as N'). An FTIR spectrum obtained for a quasi-photosteady state at 260 K showed vibration bands of water, probably due to such a structure in wild type bacteriorhodopsin (42). Actual proton transfer, however, presumably takes place in the transition state between M and N, and thus cannot be observed directly, even by time-resolved spectroscopy.

The current systematic studies provide additional information about the dynamics of internal water molecules during the bacteriorhodopsin photocycle at room temperature. Time-resolved step-scan FTIR spectra reveal light-induced changes in O–H stretching vibrational bands of water in the 3750-3500 cm<sup>-1</sup> region. The results are discussed by comparison with those from static FTIR difference spectra obtained at cryogenic temperatures.

### MATERIALS AND METHODS

### **Sample Preparation**

Bacteriorhodopsin in the form of purple membrane from  $Halobactrium\ salinarum\ S9$  was kindly provided by Sergei Balashov. A 100  $\mu$ l aliquot of bacteriorhodopsin in the purple membrane (70  $\mu$ M) supplemented with 2  $\mu$ l of phosphate buffer (0.1 M, pH 7.0) was dried under vacuum to create a spot about 12 mm in diameter in the center of a 25 mm diameter BaF2 window. The sample was then hydrated with 0.5  $\mu$ l of water (H2O, or H2<sup>18</sup>O). The space above the sample was sealed by means of a silicone rubber ring (1/32 inch thick) coated with vacuum grease, and a second 25 mm window. This stack of windows and spacer was clamped together in a flow-jacketed cell holder (Harrick, TFC-3-M25), and temperature was maintained by circulation of water at 25°C (298 K). The sample was allowed to sit in the compartment of the spectrometer for at least 3 hours before measurement. The compartment was purged continuously with nitrogen gas. The light-adapted state of bacteriorhodopsin (BR) was obtained by exposing the sample to ~2000 laser shots (equivalent to a single cycle of data acquisition; see below) immediately before the start of data acquisition. Typical samples had an absorbance of ~0.4 at 568 nm, 1.3-1.7 at 3380 cm<sup>-1</sup> and 0.8-1.1 at 1658 cm<sup>-1</sup>.

# **Data Acquisition**

Time-resolved step-scan FTIR spectra were recorded with a Varian FTS-6000 spectrometer. A photoconductive MCT detector with a dc-coupled preamplifier was used. Data were

acquired for either 10 or 20 ms in each repetition (10 Hz) with a time resolution of 5  $\mu s$  per point. The photocycle was initiated using a frequency-doubled Nd:YAG laser (Coherent Surelite I, 532 nm, duration 5 ns). The laser was fired 2 ms after the start of acquisition. Laser pulse energy at the sample was measured to be ~2.8 mJ/cm². Spectra were collected in the 3800-800 cm $^{-1}$  region (8 cm $^{-1}$  resolution, with a UDR-4 filter, Varian). The data were typically summed for 96 scans (about 3 hours) at a time. For each type of sample, several such data sets were acquired and processed together (see below).

#### Laser arrangement

Timing of the laser was controlled using a pulse generator based on a CTM-50A counter-time card (Metrabyte). The laser beam was expanded appropriately by a combination of concave and convex lenses, passed into the sample compartment, through a window, and then directed to the sample at an angle of about 25 degrees to the IR probe beam, using a laser mirror in a zero-overhang mirror mount (Thorlabs, KG1) mounted backwards. Germanium windows (25 mm diameter, 1 mm thick) with a broad-band antireflection coating (Kolmar Technologies) were used to exclude scattered laser light from the detector compartment, and to exclude the internal HeNe laser from the sample compartment.

#### **Data Processing**

After acquisition of the time resolved data, Fourier transformation was carried out using the Varian Resolution software (using NB medium apodization) and the results were saved as a single file. Subsequent processing was carried out in MATLAB (The Mathworks, Natick, MA). The effect of the cyclic 16 KHz oscillation of stationary mirror was corrected for at each repeating position of the oscillation by using average background spectra calculated from the first 2 ms (400 points) of pre-trigger data. These spectra were then used to convert the time resolved data to absorbance difference spectra (with respect to the pre-photolysis state). For bacteriorhodopsin in  ${\rm H_2}^{16}{\rm O}$ , and in  ${\rm H_2}^{18}{\rm O}$ , 44 and 27 files respectively were averaged. Finally, corrections were made for baseline drift (and in some cases for a background signal introduced when a short step-to-data acquisition delay was used with some of the older data).

A global multi-exponential fit was then applied to the data using SplMod (Provincer and Vogel, 1983; see also http://www.s-provencher.com/). Three different spectral regions were used for this. First, a fit was carried out using a matrix made up of the 2000-900 cm $^{-1}$ , 2900-2600 cm $^{-1}$ , and 3750-3600 cm $^{-1}$  regions (Fit A). Subsequently, fitting was carried out using only the 1800-900 cm $^{-1}$  region (Fit B), and then the 3750-3630 cm $^{-1}$  region (Fit C). The number of time-points (from the point of initiation by the laser flash) was reduced below 1000, with an algorithm that averages adjacent data points using a window that begins with a width of one point and increases in width as it moved up the time axis. SplMod was dimensioned to accept a matrix 512 × 1024 (frequencies × time) and was configured to try to fit functions of 1-7 exponentials, i.e.

$$A(\nu,t) = c_0(\nu) + \sum_{i=1}^{n} c_i(\nu) \exp(k_i t)$$

where n is the number of exponential components,  $\nu$  is frequency, t is time,  $k_i$  is the rate constant of the i<sup>th</sup> components,  $c_i$  is the corresponding spectrum;  $c_0$  is the spectrum of the constant component. The rate constants obtained from SplMod were used to calculate the component spectra  $c_i(\nu)$  across all frequencies in the full data set using a Gaussian elimination method (the mldivide "backslash" function of MATLAB).

### Global Fitting with Six-Exponentials

The appropriate number of exponentials for a global fit can be judged from the size of the residuals. **Figure 1** shows the average absolute value of residuals—the differences between the measured absorbance values and the fit results—calculated for the entire time range (a) and for the first 250  $\mu s$  (b) for the data obtained in  $H_2^{16}O$ . The residuals for the first 250  $\mu s$  (b), which are larger than those for the whole time range (a), decreased significantly at several frequencies in going from the five (black) to the six (red) exponential fit. However, the residuals for the seven (green) exponential fit are nearly coincident with those of the six exponential fit (b). There are very small differences in the residuals for the complete time range (a) between the five (black) and six (red) exponential fits, the latter of which is coincident with seven (green) exponential fit (a). Also the 6-fit gave results in agreement with previous published reports (see below). Thus, a six exponential function is most reasonable choice for global fitting of our current data.

# Spectra of Model Intermediates (b-spectra)

The spectra obtained in this way, together with the rate constants, were then used to calculate the spectra for a reaction consisting of a linear sequence of intermediates, using the method of Chizhov et al. (43).

**BR** is the preflash state. The transition of  $BR \to 0$  corresponds to the unresolved rapid change that accompanies the laser flash. This step is not included in the kinetic model, which begins with intermediate 0. We will refer to 0, I, II etc as "model" intermediates to distinguish them from the canonical intermediates of the bacteriorhodopsin photocycle: K, L, M etc.

The result was a difference spectrum for each transition in the reaction sequence (plus a constant spectrum). Since the original absorbance data were calculated using the unphotolyzed initial state as baseline, the spectra associated with the transitions between the model intermediates (I-minus-0, II-minus-I, etc) could be summed to obtain the spectrum of each model intermediate with respect to the unphotolyzed initial state (BR). The spectra of model intermediates obtained in this way will be referred to as **b-spectra**;  $b_1$  is the spectrum of I (the model intermediate formed in the kinetic phase with rate  $k_1$ ),  $b_2$  is the spectrum of II (the model intermediate formed in the kinetic phase with rate  $k_2$ ), and so on. The rates of the sequential processes can also be expressed as time constants ( $i_1$ ), the reciprocals of the rate constants ( $k_1$ ). Thus,  $t_1$  is the lifetime (i.e. time constants of decay) of the preceeding intermediate with spectrum  $b_{i-1}$ .

**Figure 2** shows the series of b-spectra obtained by the six exponential fit. In this spectral region (1900 to 900 cm<sup>-1</sup>), all of the spectra from films hydrated with  $H_2^{18}O$  (not shown) coincided with the spectra from films hydrated with  $H_2^{16}O$  shown in Figure 2. The spectral shapes of a series of our b-spectra are also similar to those of Rödig et al. (28). In figure 2(i), the residuals (average of absolute value of the difference between fit and data) are depicted as a pair of curves, showing the positive value of the residuals, and its negative, at each frequency. These residuals are almost negligible as compared with the appreciable bands in spectra  $b_0$  to  $b_6$ .

A large number of our time-resolved data sets were recorded with a time base extending to only 8 ms after the flash (2000 data points). In this time range, the photocycle is apparently still incomplete. Nevertheless, the first five component spectra (Figure 2, b-f) were almost identical in shape and amplitude to the corresponding b-spectra from data extending to 18

ms after the flash (4000 data points). By 18 ms the photocycle is almost complete. In what follows we will focus on the 8-ms data because our present concern is the reaction intermediates represented in spectra  $b_1$  through  $b_5$  and because we have a significantly larger quantity of data for this time scale.

# Contribution of L, M, N and O to the b-spectra

The global fitting procedure described above produced component spectra (b-spectra) for a reaction model consisting of a linear sequence of irreversible steps. These "model intermediates" are each linear combinations of the canonical bacteriorhodopsin photocycle intermediates. The contributions of the photocycle intermediates to the b-spectra in **Figure 2** were estimated from the vibrational bands characteristic of the L, M, N and O intermediates (reviewed in 44). To scale the subtraction factors between different b-spectra, the 1739 cm<sup>-1</sup> band arising from Asp96 in the L intermediate and the 1761 cm<sup>-1</sup> band arising from Asp85 in M were used with the assumption that these bands maintain a consistent shape. First of all, spectrum  $b_3$  (d) is due to pure M. The top of the 1185 cm<sup>-1</sup> band in spectrum  $b_3$  is located below the baseline, which is a defining feature of M (12), and bands characteristic of L at 983 cm<sup>-1</sup> and N at 1671 cm<sup>-1</sup> are absent.

Spectra  $b_0$  (a),  $b_1$  (b), and  $b_2$  (c) show a negative band at 1739 cm<sup>-1</sup>, which is due to the perturbations of Asp96 and Asp115 typical of L. Spectrum  $b_1$  (b) contains  $K_L$  as indicated by the presence of a positive feature at 1508 cm<sup>-1</sup> (45). The amplitude of this feature in  $b_1$  is about 30% of what it is in  $b_0$  (a), and the amplitude of the 1739 cm<sup>-1</sup> band in  $b_0$  is about 85% of that in  $b_1$ . From these results, the contribution of  $K_L$  to  $b_1$  was estimated to be about 5%. The contribution of  $K_L$  in  $b_1$  can be removed by subtracting 50% of  $b_0$ . The main contribution to spectrum  $b_1$  is from L. Spectrum  $b_1$  exhibits some intensity around 1761 cm<sup>-1</sup>, which was estimated to be about 20% of the 1761 cm<sup>-1</sup> band of  $b_3$  (d) due to M of Asp85. Subtraction of 20% of  $b_3$  from  $b_1$  leads to a positive band at 1752 cm<sup>-1</sup> due to the perturbation of Asp96 (see below Figure 5a). The positive band at 1761 cm<sup>-1</sup> due to M is pronounced in  $b_2$  (c). The intensity of this feature is about 70% of what it is in the pure M spectrum  $b_3$ . Spectrum  $b_2$  shows a negative band at 1739 cm<sup>-1</sup>, which is characteristic of L. Subtraction of 30% of  $b_1$  (L) from  $b_2$  gave the same spectral shape as  $b_3$  (M).

In b<sub>4</sub> (e) several features due to N appear; namely a slight extension of the 1761 cm<sup>-1</sup> band toward lower frequencies, with a peak at 1759 cm<sup>-1</sup>, the appearance of a negative band at 1671 cm<sup>-1</sup>, and an increase of positive bands at 1557 and 1185 cm<sup>-1</sup>. Removal of the contribution of M from b<sub>4</sub> (by subtraction of 60% of b<sub>3</sub>) results in the complete depletion of the negative band at 1661 cm<sup>-1</sup> due to M, and a shift of the 1761 cm<sup>-1</sup> band due to Asp85 toward 1756 cm<sup>-1</sup> (see below Figure 5c). Thus, spectrum b<sub>4</sub> is composed of 60% of M and 40% of N. Spectrum b<sub>5</sub> (f) exhibits a positive band at 1504 cm<sup>-1</sup> due to O (32). A smaller negative band at 1167 cm<sup>-1</sup> arises from the cancellation by the positive band at 1172 cm<sup>-1</sup> of O. This spectrum also contains a contribution from M as judged from the presence of the band at 1761 cm<sup>-1</sup>. This M would be present together with N as in b<sub>4</sub>. The composition of b<sub>5</sub> was estimated as 45% M, 47.5% N and 7.5% O. A spectrum without the contribution from M can be obtained from b<sub>5</sub> by subtracting 75% of b<sub>4</sub> from b<sub>5</sub>. The resulting spectrum (g) shows the characteristics of O more clearly; especially positive bands at 1507 and 1172 cm<sup>-1</sup>, the latter as a shoulder (g). The content of O in this spectrum is estimated to be about 30% by comparison of the amplitude ratio of the 1507 cm<sup>-1</sup> band to that of the 1556 cm<sup>-1</sup> band in the pure O-minus-BR spectrum (32). The rest (70%) should be due to N. This spectrum is identical to that obtained by exchanging the order of the last two time constants (k<sub>5</sub> and k<sub>6</sub>, in our case) as proposed by Chizhov et al. (43), and similar to the penultimate spectrum shown in Figure 3A of Rödig et al. (28). Spectrum b<sub>6</sub> (h) is roughly similar to b<sub>5</sub> (f) in shape, but with only one sixth the amplitude. This is probably the sum of a b<sub>5</sub>-like

spectrum with a spectrum that has a nearly mirror-image shape (restoration of the initial BR state from the last step of the photocycle). It is very similar to the final spectrum shown by Rödig et al. (28). We plan to discuss this spectrum in a separate publication.

The L-minus-BR and N-minus-BR spectra calculated in this analysis (see below Figure 5a, c) and the M-minus-BR spectrum of  $b_3$  (Figure 2d) are nearly identical in the 1800-1100 cm<sup>-1</sup> region with those obtained from the factor analysis by Heßling et al. (32).

#### **RESULTS**

### Results of the six-component fit

The first time constant obtained from our data,  $\tau_1$ , which is the lifetime of the unresolved zero-time component ( $b_0$ ) is typically 2-3  $\mu s$ . Since this is shorter than our time-resolution (5  $\mu s$  per point), it cannot be considered a real measured lifetime. We will therefore begin our discussion of the kinetics of the photocycle with  $\tau_2$ , which is the lifetime (decay time constant) of  $b_1$ , and following this convention, generally refer to time constants as the lifetimes of specific intermediates.

The lifetimes ( $\tau_2$  - $\tau_6$ ) in  $H_2^{16}O$  for  $b_1$ ,  $b_2$ ,  $b_3$ ,  $b_4$ , and  $b_5$ , 43  $\mu$ s, 130  $\mu$ s, 525  $\mu$ s, 1.5 ms, and 6.1 ms, respectively, are almost coincident with the corresponding values in  $H_2^{18}O$  (48  $\mu$ s, 160  $\mu$ s, 570 $\mu$ s, 1.8 ms, and 5.5 ms, respectively). The lifetimes of these components are similar to the corresponding values obtained with similar hydrated films by Rödig et al. (25) of 40  $\mu$ s, 134  $\mu$ s, 544  $\mu$ s, 1.6 ms and 5 ms, respectively. The lifetimes determined by these FTIR studies are also similar to results from visible spectroscopic measurements on purple membranes in solution reported by Chizhov et al. (39) of 30  $\mu$ s, 100  $\mu$ s, 500  $\mu$ s, 1.5 ms, and 5 ms.

We will discuss a set of five b-spectra ( $b_1$  to  $b_5$ ) obtained by global analysis of the time-resolved FTIR difference spectra at pH 7 (**Figure 2**). Comparison with static spectra of the canonical bacteriorhodopsin intermediates allows these component spectra to be further analyzed. We concluded above that  $b_1$  (b) is 75% L with 5%  $K_L$  and 20% M;  $b_2$  (c) is 70% M with 30% L;  $b_3$  (d) is 100% M;  $b_4$  (e) is 60% of M and 40% of N; and  $b_5$  (f) is 45% M and 47.5% N with 7.5% O (see Materials and Methods).

# Broad Water O-H Vibrational Feature in the 3750-3500 cm<sup>-1</sup> Region

**Figure 3** compares  $b_1$  (a),  $b_2$  (b),  $b_3$  (c),  $b_4$  (d), and  $b_5$  (e) in the 3750-3500 cm<sup>-1</sup> region for films hydrated with  $H_2^{16}O$  (solid lines) and  $H_2^{18}O$  (broken lines). In  $b_1$  (a) this spectral region is dominated by a broad positive feature centered near 3610 cm<sup>-1</sup>. The amplitude of this broad peak decreases from  $b_1$  (a) to  $b_2$  (b). Some intensity remains in  $b_3$  (c) which does not contain any contribution from L, but this feature seems to have disappeared entirely in  $b_4$  (d) and  $b_5$  (e) with the appearance of N and O. In all cases, the spectra in  $H_2^{16}O$  are more intense than those in  $H_2^{18}O$  at frequencies above 3610 cm<sup>-1</sup> and less intense at frequencies below 3610 cm<sup>-1</sup>. This indicates that a large part of the broad feature is due to water O–H stretching vibrations. The L-*minus*-BR spectrum at 170 K (g) exhibits a broad positive feature in the 3550-3450 cm<sup>-1</sup> region (10) (**Figure 3** does not show the region below 3500 cm<sup>-1</sup>). No corresponding feature is observed in the same frequency region of spectrum  $b_1$ , which is mainly due to L at 298 K (a). Note that the feature in the 170 K spectrum is larger in amplitude than the averaged residuals from the time-resolved spectra (f) indicating that if this feature was present in the time-resolved spectra, it would be observable.

# Vibrational Bands at 3670, 3657, and 3645 cm<sup>-1</sup>

Onto this broad feature, a number of sharp positive and negative bands are superimposed. Among them are positive bands at 3670 and 3657 cm<sup>-1</sup> and a negative band at 3645 cm<sup>-1</sup>. These bands are observed in a region where the residuals are significantly smaller. Corresponding bands are observed in H<sub>2</sub><sup>18</sup>O at 3657, 3645 and 3634 cm<sup>-1</sup>, respectively, showing that these bands arise from water O–H stretching vibrations. As judged from their location at higher frequencies, the water O–H bonds, responsible for these bands, have no H-bonding partners.

The negative band at  $3645 \text{ cm}^{-1}$  corresponds to the band at  $3642 \text{ cm}^{-1}$  in the L-minus-BR spectrum at 170 K (g). It can be recognized in all the five spectra (a-e) as a dip with similar intensity irrespective of composition of the intermediates. Thus the disappearance of the water O–H vibration band is constant through intermediates L, M and N.

#### Perturbations of Water in M and N

The two positive bands at 3670 and 3657 cm<sup>-1</sup> are observed in spectrum  $b_3$  (c) which is due to 100% M. Both bands are also present in  $b_2$  (b) which is 70% M and  $b_4$  (d) which is 60% M. The 3670 cm<sup>-1</sup> band decreases in intensity in  $b_5$  (e), consistent with a decrease in the contribution of M to 45% in this spectrum. These results suggest that the 3670 cm<sup>-1</sup> band is due to M. The 3657 cm<sup>-1</sup> band persists in  $b_4$  (d) and  $b_5$  (e) suggesting that this band may also be exhibited by the N intermediate. We cannot judge whether these bands are present in O because this intermediate makes only a very small contribution to  $b_5$ . The same trends can be observed in the corresponding shifted bands in  $H_2^{18}O$  (dotted lines) at 3657 and 3645 cm<sup>-1</sup>.

# The Broad Water Vibration Feature Changes in Concert with the L-to-M Transition

The broad feature of water vibrations is expected to be intimately correlated with L, in the same manner as similar bands of L at 170 K (Figure 3g). It is important to distinguish whether the spectral changes in these water vibrations take place in concert with the L-to-M transition, or whether this apparent linkage is the result of the global fit being driven by the larger absorbance bands and lower noise in the 1800-900 cm<sup>-1</sup> region. This was examined by comparing an independent fit to only the 3750-3630 cm<sup>-1</sup> region (Fit C) to the results of a fit to only the 1800-900 cm<sup>-1</sup> region (Fit B). The 3750-3630 cm<sup>-1</sup> region was selected because the residuals were smaller than below 3630 cm<sup>-1</sup>. The spectral shapes and the time constants for Fit B are almost completely coincident with the results which were obtained by fitting to both regions (Fit A; Figure 3), indicating that the same underlying kinetics are driving changes in the vibration bands in the 1800-900 cm<sup>-1</sup> region due to the chromophore and the protein and also those in the 3750-3630 cm<sup>-1</sup> region due to water. As shown in Figure 4 the shapes of spectra b<sub>1</sub> (blue) and b<sub>2</sub> (red) in a five exponential fit of the Fit C spectral region are almost exactly coincident with those of spectra b<sub>1</sub> (dotted line; blue) and b<sub>2</sub> (dotted line, red) of Fit B (6-exponential fit). The lifetime <sub>2</sub> from Fit C (38 μsec) is also similar to that from Fit B (43 µsec). Together, these results strongly indicate that the water structural changes that give rise to the broad band are related to the L-to-M transition.

#### Perturbations of the Schiff base and Asp96

Previously Rödig et al. (28) have shown that the Schiff base HOOP band of L at room temperature is located at 983 cm<sup>-1</sup>, while Maeda et al. (27) have shown that the 1074, 1065 and 1057 cm<sup>-1</sup> bands of L at 170 K are due to the HOOP bands of the Schiff base. **Figure 5** shows an L-*minus*-BR spectrum (a) that was obtained by subtracting the M-*minus*-BR spectrum (20% of  $b_3$ ) and the contribution of  $K_L$  (50% of  $b_0$ ) from  $b_1$  as described above, together with the L-*minus*-BR spectrum at 170 K (b). The spectrum at 170 K was obtained

as described previously (27). The bands due to the retinal at 1202 and 1168 cm<sup>-1</sup> are similar in the two spectra. The larger bandwidth of these bands at 298 K (a) could be due to the fact that this spectrum was recorded at a resolution of 8 cm<sup>-1</sup> whereas the spectrum at 170 K (b) was recorded at 2 cm<sup>-1</sup>. The HOOP band of L at 298 K can be observed as a wide band with a peak at 984 cm<sup>-1</sup> (a), but the three HOOP bands observed in the spectra taken at 170 K around 1065 cm<sup>-1</sup> (b) are not seen in the room temperature spectrum (a). In the spectrum of L at 170 K (b), there are two bands arising from the Schiff base in-plane bending vibrations, at 1312 and 1300 cm<sup>-1</sup> (46). In the spectrum at 298 K (a) the former peak has disappeared while the latter has intensified. Another in-plane bending vibration band of the Schiff base has shifted but retained its shape, moving from 1400 cm<sup>-1</sup> at 170 K (b) to 1395 cm<sup>-1</sup> at 298 K (a). These differences are clearly real in spite of the different frequency resolutions. The out-of-plane and in-plane bending vibration bands of the Schiff base at 298 K are located at lower frequencies than those at 170 K. This indicates weaker H-bonding of the Schiff base in L at 298 K than at 170 K.

The vibrational features of the Schiff base of L at room temperature are rather similar to those observed in the N-minus-BR spectrum (c) at room temperature, that was obtained from the current results by subtracting the M-minus-BR spectrum (60% of  $b_3$ ) from  $b_4$ . The intense 1300 cm<sup>-1</sup> band of L at room temperature (a) is similar to that of N at 1302 cm<sup>-1</sup> (c). On initial inspection, the HOOP band of N might appear to be missing. However, the absence of the negative band at 1005 cm<sup>-1</sup> in the N-minus-BR spectrum must be due to cancellation by the HOOP band of N at around 1005 cm<sup>-1</sup>. The HOOP band at 984 cm<sup>-1</sup> in the spectrum of L at 298 K (a) is much closer in frequency to this HOOP band of N (c) than to the HOOP bands of L at 170 K (b). Thus, at 298 K the environment of the Schiff base of L is similar to that of N.

The negative band at 1739 cm<sup>-1</sup> in the spectrum at 170 K is actually composed of two bands due to Asp96 and Asp115 at 1743 cm<sup>-1</sup> and 1736 cm<sup>-1</sup> respectively (Figure 5b; 5, 9). Corresponding bands can also be seen in the spectra at 298 K (a). The C=O stretching band of Asp96 in the L intermediate at 170 K is observed as a positive feature at 1748 cm<sup>-1</sup> (b). In the L-minus-BR spectrum at 298 K only a diffuse band with a much smaller intensity than the 1748 cm<sup>-1</sup> band was observed at 1752 cm<sup>-1</sup> (a). In the previous papers clear bands were not observed in this region (32, 47). Nevertheless, the possibility that Asp96 is deprotonated is small because a band similar to the 1403 cm<sup>-1</sup> band of N (c) due to deprotonated Asp96 (10) is not detected around 1400 cm<sup>-1</sup> (a). Thus, Asp96 undergoes a perturbation in L at 298 K but in a different way from that at 170 K.

### DISCUSSION

The time-resolved FTIR spectral changes that occur during the bacteriorhodopsin photocycle contain a number of features that are due to perturbations of internal water molecules, further emphasizing the critical functional roles of water. It is important that any absorption bands assigned as being due to water vibrations, either individual molecules or clusters, be verified by observing the frequency shift due to exchange of  $\mathrm{H_2^{18}O}$  for  $\mathrm{H_2^{16}O}$ .

### Water Forms H-bonds with Asp85 in L, M, and N at 298 K

A water vibrational band is observed as a trough in the L-minus-BR and M-minus-BR spectra at 3645 cm $^{-1}$ . This feature which was initially discovered in studies of L at 170 K and M at 230 K (48) is observed as a depletion band upon formation of L at 298 K, and this feature persists in M and N. This band is also the same one that was recently detected in static difference spectra, obtained using an *in situ*  $H_2^{16}O/H_2^{18}O$  exchange technique with BR at room temperature (37). In the  $H_2^{16}O/H_2^{18}O$  exchange measurements, the band was not observed in D85N (37) and it was also not observed in the light-induced difference

spectrum of the D85N mutant at 170 K (25). As discussed previously (37, 49) this water vibration is very likely due to the free O–H bond of Wat401 in BR, a water whose other hydrogen interacts with Asp85 (i.e., Asp85-COO<sup>-••</sup>H–O–H), as is seen in the crystal structure of BR (50). The present study shows that one O–H bond that does not form an H-bond in BR subsequently forms an H-bond in L, M and N under physiological conditions. Evidence for the interaction of this water O–H group with Asp85 in M has previously been presented by FTIR and crystallographic studies (23, 26).

### Changes in water molecules are Coordinated with the L-to-M Transitions at 298 K

Previous studies at 170 K showed that there are water vibrational bands in the 3550-3450 cm<sup>-1</sup> region that appear in the L state (48). Mutational studies have suggested that the water molecules in question are present in L at 170 K as a cluster between the Schiff base and Asp96 (27, 51). Similar vibrational bands of water were also shown to be present in N at 260 K (42). In the time-resolved room temperature results, this set of features due to water bands at 170 K is replaced by a broad water vibrational feature in the 3750-3500 cm<sup>-1</sup> region. A large part of this feature disappears in the two step L-to-M transition characterized by 2 (43 μs) and 3 (0.13 ms), but a small part remains until the formation of N (4; 0.53 ms). Garczarek et al. (35) observed similarly decaying vibrational features in the 3000-1800 cm<sup>-1</sup> region by using a visible light-absorbing dye. These features decayed with a time constant of 300 µs roughly similar to our results. Part of the broad water vibrational feature is ascribable to heat emitted from the excited state chromophore. However, the decay of this broad water vibrational feature in spectra b<sub>1</sub> and in b<sub>2</sub> of Fit C is kinetically coordinated with structural changes of the chromophore and the protein in the L-to-M transition. Thus these changes in water molecules observed for the vibrations in the 3750-3630 cm<sup>-1</sup> region cannot be independent of the L-to-M transition, and the waters must be accommodated within a specific structure for L. Free energy associated with relaxation of the light-activated chromophore in the course of the bacteriorhodopsin photocycle may facilitate assembly of the water cluster, which exhibits the broad vibrational feature of water.

In our bacteriorhodopsin samples about 4000 water molecules are present for each molecule of bacteriorhodopsin (0.5  $\mu$ l of water vs 180  $\mu$ g of bacteriorhodopsin). The maximum absorbance change of the feature in the 3750-3630 cm<sup>-1</sup> region is about ~0.001 which corresponds to 0.1% of the total number of water molecules. Hence, the number of water molecules involved is more than 4, but not a large number (for example ~10), even if we assume a relatively small molar extinctions for weakly H-bonding water on the basis of the fact that the water vibration bands that we observe are located at higher frequencies (with weaker H-bonding) than environmental water whose vibrations appear around 3350 cm<sup>-1</sup>. This feature could thus arise entirely from internal water molecules. When we observe changes in water molecules that are accommodated in an internal cavity in the protein associated with an intermediate, they can arise either due to heating from the chromophore or by reorganization of water molecules in situ that changes the geometry and strength of H-bonds, or some combination of both effects. Even if some part of a water band is produced by heat, the important result here is that there are water molecules that change in concert with the L-to-M transition.

Thus in the L intermediate at 298 K there are perturbations of water, though the H-bonds are weaker than in the water cluster at 170 K. Perturbations of the Schiff base and Asp96 are also observed at 298 K, though in different ways than at 170 K. The environment of the Schiff base in L is rather similar to that in N, where the Schiff base interacts with water (42). Thus a structured water network between the Schiff base and Asp96 also may be present at room temperature, but as a rigidly organized structural element.

# Water Molecules in the Phe219-Thr46-Asp96 Region in M

Previous studies at 230 K have found that the water vibration band of M at 3671 cm<sup>-1</sup> was affected by F219L and T46V, while the corresponding band of N at 3654 cm<sup>-1</sup> was affected by V49A (52). To explain these results, it was proposed that water molecules are present in M in the region around Thr46-Phe219 and that in N some of them have moved to the region around Val49 and the Schiff base. A crystallographic structure of M from a sample in which the intermediate was produced at room temperature and then cooled to 100 K for diffraction studies (23), shows two water molecules in a cavity surrounded by Phe219, Trp182, Leu93, Thr46 and Thr178 (**Figure 6**). This non-polar cavity is on the cytoplasmic side of bacteriorhodopsin near Asp96, but no water molecules were detected on the cytoplasmic side in the neighborhood of the Schiff base.

### Water Networks between the Schiff Base and Asp96 in L and M

The T46V mutant, which eliminates the water vibrations associated with this water cluster in the L state at cryogenic temperatures, results in a shift of equilibrium between L and M to favor the M state at room temperature (53). The T46V/D96N double mutant restores the water vibrations at 170 K and also restores the equilibrium between L and M back towards the L intermediate. It is reasonable to propose that at room temperature Thr46 and Asp96 are involved in a specific structure involving the local water cluster and that perturbing this water network alters the equilibrium between the L and M intermediates.

Neutron scattering studies on purple membrane by the Zaccai group (54, 55) have shown that the ability of the bacteriorhodopsin pigment to enter a functionally relaxed state is correlated with the presence of an environment in which large amplitude atomic motions are possible. Such an environment was described as "soft," and shown to occur above 230 K for the hydrated bacteriorhodopsin in purple membrane. The present results show that vibrational bands due to water molecules and the Schiff base in L at room temperature are different from those at 170 K where the protein environment does not allow transformation of the rigid structure of water interacting with the Schiff base into the M state where the structure is quite different. Water molecules in L are present in the region surrounded by the relatively apolar residues, Val49, Leu93, and Trp182 in addition to the Schiff base, Thr46 and Asp96. In the L-to-M transition at room temperature, water relocates, not through changes in direct H-bonding, but as a mobile spacer with structured interactions in a relatively soft environment.

# **Acknowledgments**

Authors are grateful to Thomas Ebrey for his critical reading of the manuscript and valuable suggestions, and Andrei Dioumaev and David Drapcho for their advice on the time-resolved system. Lay Min Lee for collegial help with the instrument, and the team at the Chemical Sciences Machine Shop at the University of Illinois, Urbana/Champaign, for their constant helpfulness and excellent work.

### **REFERENCES**

- (1). Lozier RH, Bogomolni RA, Stoeckenius W. Bacteriorhodopsin: A light-driven proton pumping in *Halobacteirum halobium*. Biophys. J. 1975; 15:955–962. [PubMed: 1182271]
- (2). Xie A,H, Nagle JF, Lozier RH. Flash spectroscopy of purple membrane. Biophys. J. 1987; 51:627–635. [PubMed: 3580488]
- (3). Sasaki J, Yuzawa T, Kandori H, Maeda A, Hamaguchi H. Nanosecond time-resolved infrared spectroscopy distinguishes two K species in the bacteriorhodopsin photocycle. Biophys. J. 1995; 68:2073–2080. [PubMed: 7612850]

(4). Váró G, Lanyi JK. Kinetics and spectroscopic evidence for an irreversible step between deprotonation and reprotonation of the Schiff base in the bacteriorhodopsin photocycle. Biochemistry. 1991; 30:5008–5015. [PubMed: 1645187]

- (5). Braiman MS, Mogi T, Marti T, Stern LJ, Khorana HG, Rothschild KJ. Vibrational spectroscopy of bacteriorhodopsin mutants: Light-driven proton transport involves protonation changes of aspartic acid residues 85, 96 and 212. Biochemistry. 1988; 27:8516–8520. [PubMed: 2851326]
- (6). Gerwert K, Souvignir G, Hess B. Simultaneous monitoring of light-induced changes in protein side-group protonation, chromophore isomerization, and backbone motion of bacteriorhodopsin by time-resolved Fourier transform infrared spectroscopy. Proc. Natl Acad. Sci. USA. 1990; 87:9774–9778. [PubMed: 11607137]
- (7). Zimányi L, Váró G, Chang M, Ni B, Needleman R, Lanyi JK. Pathways of proton release in the bacteriorhodopsin photocycle. Biochemistry. 1992; 31:8535–8543. [PubMed: 1327104]
- (8). Balashov SP, Imasheva ES, Ebrey TG, Chen Y, Menick DR, Crouch RK. Glutamate-194 to cysteine mutation inhibits fast light-induced proton release in bacteriorhodopsin. Biochemistry. 1997; 36:8671–8676. [PubMed: 9289012]
- (9). Gerwert K, Hess B, Soppa J, Oesterhelt D. Role of aspartate-96 in proton translocation by bacteriorhodopsin. Proc. Natl. Acad. Sci. USA. 1989; 86:4943–4947. [PubMed: 2544884]
- (10). Maeda A, Sasaki J, Shichida Y, Yoshizawa T, Chang M, Ni B, Needleman R, Lanyi JK. Structures of aspartic acid-96 in the L and N intermediates of bacteriorhodopsin: Analysis by Fourier transform infrared spectroscopy. Biochemistry. 1992; 31:4684–4690. [PubMed: 1316157]
- (11). Smith SO, Pardoen JA, Mulder PPJ, Curry B, Lugtenburg J, Mathies R. Chromophore structure in bacteriorhodopsin's O<sub>640</sub> photointermediate. Biochemistry. 1983; 22:6141–6148.
- (12). Souvignir G, Gerwert K. Proton uptake mechanism of bacteriorhodopsin as determined by time-resolved stroboscopic-FTIR- spectroscopy. Biophys. J. 1992; 63:1393–1405. [PubMed: 19431858]
- (13). Balashov SP, Lu M, Imasheva ES, Govindjee R, Ebrey TG, Othersen B III, Chen Y, Crouch RK, Menick DR. The proton release group of bacteriorhodopsin controls the rate of the final step of its photocycle at low pH. Biochemistry. 1999; 38:2026–2039. [PubMed: 10026285]
- (14). Luecke H, Schobert B, Richter H-T, Cartailler J-P, Lanyi JK. Structural changes in bacteriorhodopsin during ion transport at 2 angstrom resolution. Science. 1999; 286:255–260. [PubMed: 10514362]
- (15). Luecke H, Schobert B, Cartailler J-P, Richter H-T, Rosengarth A, Needleman R, Lanyi JK. Coupling photoisomerization of retinal to directional transport in bacteriorhodopsin. J. Mol. Biol. 2000; 300:1237–1255. [PubMed: 10903866]
- (16). Sass HJ, Büldt G, Gessenich R, Hehn D, Neff D, Schlessinger R, Berendzen J, Ormos P. Structural alterations for proton translocation in the M state of wild-type bacteriorhodopsin. Nature. 2000; 406:649–653. [PubMed: 10949308]
- (17). Facciotti MT, Rouhani S, Burkard FT, Betancourt FM, Downing KH, Rose RB, McDermott G, Glaeser RM. Structure of an early intermediate in the M-state phase of the bacteriorhodopsin photocycle. Biophys. J. 2001; 81:3422–3455. [PubMed: 11721004]
- (18). Schobert B, Brown LS, Lanyi JK. Crystallographic structures of the M and N intermediates of bacteriorhodopsin: Assembly of a hydrogen-bonded chain of water molecules between Asp-96 and the retinal Schiff base. J. Mol. Biol. 2003; 330:553–570. [PubMed: 12842471]
- (19). Lanyi JK, Schobert B. Crystallographic structure of the retinal and the protein after deprotonation of the Schiff base: The switch in the bacteriorhodopsin photocycle. J. Mol. Biol. 2002; 321:727–737. [PubMed: 12206786]
- (20). Lanyi JK, Schobert B. Mechanism of proton transport in the bacteriorhodopsin from crystallographic structures of the K, L, M<sub>1</sub>, M<sub>2</sub> and M<sub>2</sub>' intermediates of the photocycle. J. Mol. Biol. 2003; 328:439–450. [PubMed: 12691752]
- (21). Edman K, Royant A, Larsson G, Jacobson F, Taylor T, van der Spoel D, Landau EM, Pebye-Peyroula E, Neutze R. Deformation of helix C in the low temperature L-intermediate of bacteriorhodopsin. J. Biol. Chem. 2004; 279:2147–2158. [PubMed: 14532280]

(22). Kouyama, Nishikawa T, Tokuhisa T, Okamura H. Crystal structure of the L intermediate of bacteriorhodopsin: Evidence for vertical translocation of a water molecule during the proton pumping cycle. J. Mol. Biol. 2004; 335:531–546. [PubMed: 14672661]

- (23). Takeda K, Matsui Y, Kamiya N, Adachi S, Okumura H, Kouyama T. Crystal structure of the M intermediate of bacteriorhodopsin: Allosteric structural changes mediated by sliding movement of a transmembrane helix. J. Mol. Biol. 2004; 341:1023–1037. [PubMed: 15328615]
- (24). Maeda A, Morgan JE, Gennis RB, Ebrey TG. Water as a cofactor in the unidirectional light-driven proton transfer steps in bacteriorhodopsin. Photochem. Photobiol. 2006 in press.
- (25). Maeda A, Sasaki J, Yamazaki Y, Needleman R, Lanyi JK. Interaction of aspartate-85 with a water molecule and the protonated Schiff base in the L intermediate of bacteriorhodopsin: A Fourier transform infrared spectroscopic study. Biochemistry. 1994; 33:1713–1717. [PubMed: 8110773]
- (26). Maeda A, Tomson FL, Gennis RB, Kandori H, Ebrey TG, Balashov SP. Relocation of internal bound water in bacteriorhodopsin during the photoreaction of M at low temperature: an FTIR study. Biochemistry. 2000; 39:10154–10162. [PubMed: 10956004]
- (27). Maeda A, Balashov SP, Lugtenburg J, Verhoeven MA, Herzfeld J, Belenky M, Gennis RB, Tomson FL, Ebrey TG. Interaction of internal water molecules with the Schiff base in the L intermediate of the bacteriorhodopsin photocycle. Biochemistry. 2002; 41:3803–3809. [PubMed: 11888299]
- (28). Rödig C, Chizov I, Weidlich O, Siebert F. Time-resolved step-scan Fourier transform infrared spectroscopy reveals differences between early and late M intermediates of bacteriorhodopsin. Biophys. J. 1999; 76:2687–2701. [PubMed: 10233083]
- (29). Iwasa T, Tokunaga F, Yoshizawa T. A new pathway in the photoreaction cycle of transbacteriorhodopsin and the absorption spectra of its intermediates. Biophys. Struct. Mech. 1980; 6:253–270.
- (30). Kalisky O, Ottolenghi M, Honig B, Korenstein R. Environmental effects on formation and photoreaction of the M412 photoproduct of bacteriorhodopsin: Implications for the mechanism of proton pumping. Biochemistry. 1981; 20:649–655. [PubMed: 7213600]
- (31). Braiman M, Bousché O, Rothschild K. Protein dynamics in the bacteriorhodopsin photocycle: Submillisecond Fourier transform infrared spectra of the L, M, and N photointermediates. Proc. Natl. Acad. Sci. USA. 1991; 88:2388–2392. [PubMed: 2006176]
- (32). Heßling B, Souvignier G, Gerwert K. A model-independent approach to assigning bacteriorhodopsin's intramolecular reactions to photocycle intermediates. Biophys. J. 1993; 65:1929–1941. [PubMed: 8298022]
- (33). Rammelsberg R, Huhn G, Lübben M, Gerwert K. Bacteriorhodopsin's intramolecular protonrelease pathway consists of a hydrogen-bonded network. Biochemistry. 1998; 37:5001–5009. [PubMed: 9538019]
- (34). Zscherp C, Schlessinger R, Tittor J, Oesterhelt D, Heberle J. In situ determination of transient pK<sub>a</sub> changes of internal amino acids of bacteriorhodopsin by using time-resolved attenuated total reflection Fourier transform infrared spectroscopy. Proc. Natl. Acad. Sci. USA. 1999; 96:5498– 5503. [PubMed: 10318912]
- (35). Garczarek F, Wang J, El-Sayed MA, Gerwert K. The assignment of the different infrared continuum absorbance changes observed in the 3000-1800 cm<sup>-1</sup> region during the bacteriorhodopsin photocycle. Biophys. J. 2004; 87:2676–2682. [PubMed: 15298873]
- (36). Garczarek F, Brown LS, Lanyi JK, Gerwert K. Proton binding within a membrane protein by a protonated water cluster. Proc. Natl. Acad. Sci. USA. 2005; 102:3633–3638. [PubMed: 15738416]
- (37). Garczarek F, Gerwert K. Functional waters in intraprotein proton transfer monitored by FTIR difference spectroscopy. Nature. 2006; 439:109–112. [PubMed: 16280982]
- (38). Zundel G. Hydrogen bonds with large proton polarizability and proton transfer processes in electrochemistry and biology. Adv. Chem. Phys. 2000; 111:1–217.
- (39). Le Courte J, Tittor J, Oesterhelt D, Gerwert K. Experimental evidence for hydrogen-bonded network proton transfer in bacteriorhodopsn shown by Fourier transform infrared spectroscopy using azide as catalysis. Proc. Natl. Acad. Sci. USA. 1995; 92:4962–4966. [PubMed: 7761432]

(40). Headrick JM, Diken EG, Walters RS, Hammer NI, Christe RA, Cui J, Myshakin EM, Duncan MA, Johnson MA, Jordan KD. Science. 2005; 308:1765–1769. [PubMed: 15961665]

- (41). Cao Y, Váró G, Chang M, Ni B, Needleman R, Lanyi JK. Water is required for proton transfer from aspartate-96 to the bacteriorhodopsin Schiff base. Biochemistry. 1991; 30:10972–10979. [PubMed: 1657155]
- (42). Maeda A, Gennis RB, Balashov SP, Ebrey TG. Relocation of water molecules between the Schiff base and the Thr46-Asp96 region during light-driven unidirectional proton transport by bacteriorhodopsin: An FTIR study of the N intermediate. Biochemistry. 2005; 44:5960–5968. [PubMed: 15835885]
- (43). Chizhov I, Chernavskii DS, Engelhard M, Mueller K-H, Zubov BV, Hess B. Spectrally silent transitions in the bacteriorhodopsin photocycle. Biophys. J. 1996; 71:2329–2345. [PubMed: 8913574]
- (44). Maeda A. Application of FTIR spectroscopy to the structural study on the function of bacteriorhodopsin. Isr. J. Chem. 1995; 35:387–400.
- (45). Maeda A, Verhoeven MA, Lugtenburg J, Gennis RB, Balashov SP, Ebrey TG. Water rearrangement around the Schiff base in the late K (K<sub>L</sub>) intermediate of the bacteriorhodopsin photocycle. J. Phys. Chem. B. 2004; 108:1096–1101.
- (46). Maeda A, Sasaki J, Pfefferlé J-M, Shichida Y, Yoshizawa T. Fourier transform infrared spectral studies on the Schiff base mode of all-trans bacteriorhodopsin and its photointermediates, K and L. Photochem. Photobiol. 1991; 54:911–921.
- (47). Chen W-G, Braiman MS. kinetic analysis of time-resolved infrared difference spectra of the L and M intermediates of bacteriorhodopsin. Photochem. Photobiol. 1991; 54:905–910.
- (48). Maeda A, Sasaki J, Shichida Y, Yoshizawa T. Water structural changes in the bacteriorhodopsin photocycle: Analysis by Fourier-transform infrared spectroscopy. Biochemistry. 1992; 31:462–467. [PubMed: 1731905]
- (49). Hayashi S, Tajikhorshid E, Kandori H, Schulten K. Role of hydrogen-bond in energy storage of bacteriorhodopsin's light-driven proton pump revealed by ab initio normal-mode analysis. J. Am. Chem. Soc. 2004; 126:10516–12517. [PubMed: 15327290]
- (50). Luecke H, Schobert B, Richter H-T, Cartailler J-P, Lanyi JK. Structure of bacteriorhodopsin at 1.55 A resolution. J. Mol. Biol. 1999; 291:899–911. [PubMed: 10452895]
- (51). Maeda A, Herzfeld J, Belenky M, Needleman R, Gennis RB, Balashov SP, Ebrey TG. Water-mediated hydrogen-bonded network on the cytoplasmic side of the Schiff base of the L photointermediate of bacteriorhodopsin. Biochemistry. 2003; 42:14122–14129. [PubMed: 14640679]
- (52). Yamazaki Y, Kandori H, Needleman R, Lanyi JK, Maeda A. Interaction of the protonated Schiff base with the peptide backbone of valine 49 and the intervening water molecule in the N photointermediate of bacteriorhodopsin. Biochemistry. 1998; 37:1559–1564. [PubMed: 9484226]
- (53). Yamazaki Y, Hatanaka M, Kandori H, Sasaki J, Karstens WFJ, Raap J, Lugtenburg J, Bizounok M, Herzfeld J, Needleman R, Lanyi JK, Maeda A. Water structural changes at the proton uptake site (the Thr46-Asp96 domain) in the L intermediate of bacteriorhodopsin. Biochemistry. 1995; 34:7088–7093. [PubMed: 7766618]
- (54). Ferrand M, Dianoux AJ, Petry W, Zaccai G. Thermal motions and function of bacteriorhodopsin in purple membranes: Effects of temperature and hydration studied by neutron scattering. Proc. Natl. Acad. Sci. USA. 1993; 90:9668–9672. [PubMed: 8415760]
- (55). Zaccai G. How soft is a protein? A protein dynamics force constant measured by neutron scattering. Science. 2000; 288:1604–1607. [PubMed: 10834833]

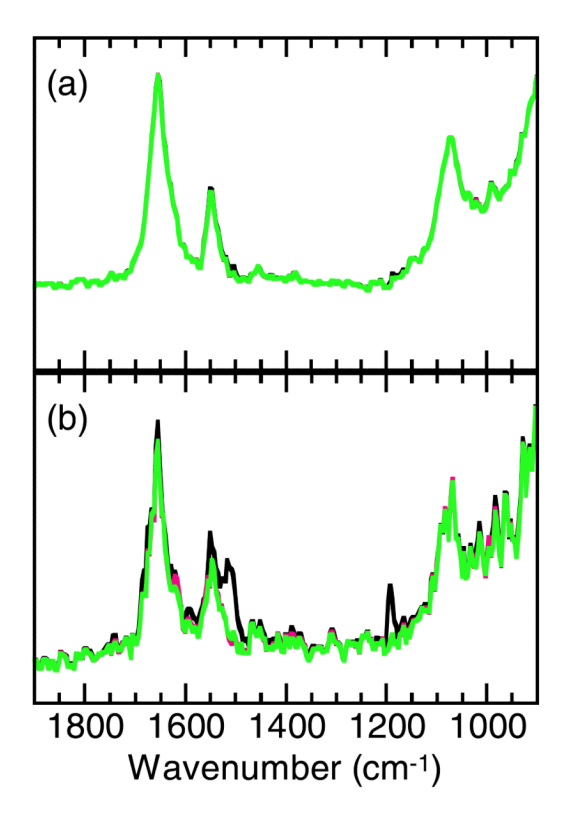


**Figure 1.** Averaged absolute value of residuals for the spectra obtained by fitting of five (black), six (red), and seven (green) exponentials. (a) Residuals averaged for the whole time range to 8 ms (1600 data points). (b) Residuals averaged for the first 250  $\mu$ s (50 data points) after the start of the photoreaction. The full length of the ordinate corresponds to 0.00007 AU.

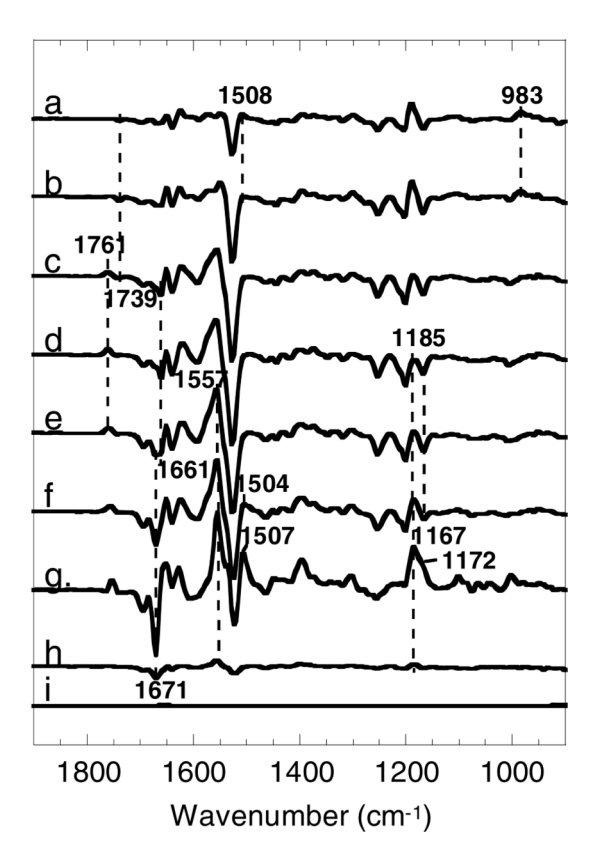


Figure 2. Model spectra obtained by a six exponential fit for bacteriorhodopsin in  $H_2^{16}O$ . (a)  $b_0$ . (b)  $b_1$ . (c)  $b_2$ . (d)  $b_3$ . (e)  $b_4$ . (f)  $b_5$ . (g) Spectrum obtained by subtracting 75% of  $b_4$  from  $b_5$ , removing the contribution of M, and resulting in enrichment of the O intermediate. (h)  $b_6$ . (i) The absolute value of the residuals averaged for the whole time range. The full length of the ordinate corresponds to 0.045 AU.

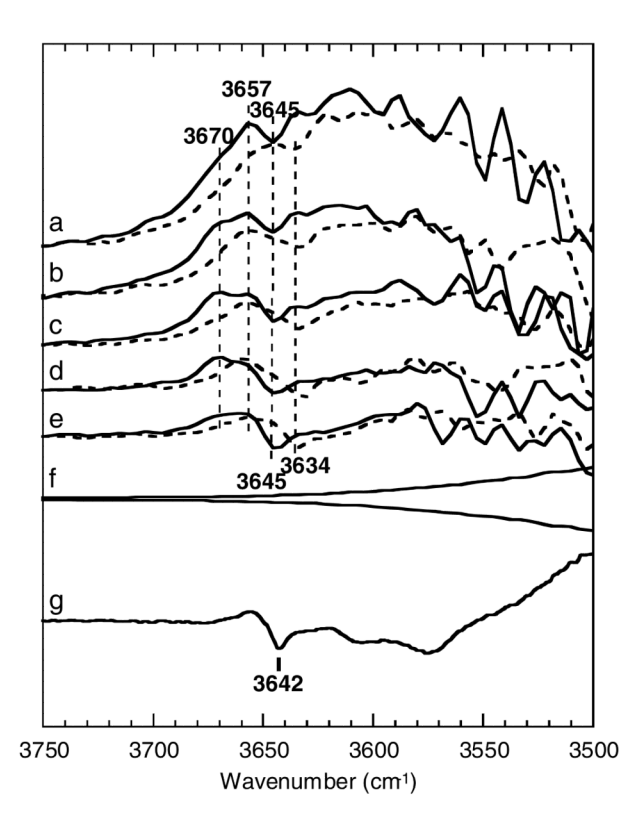
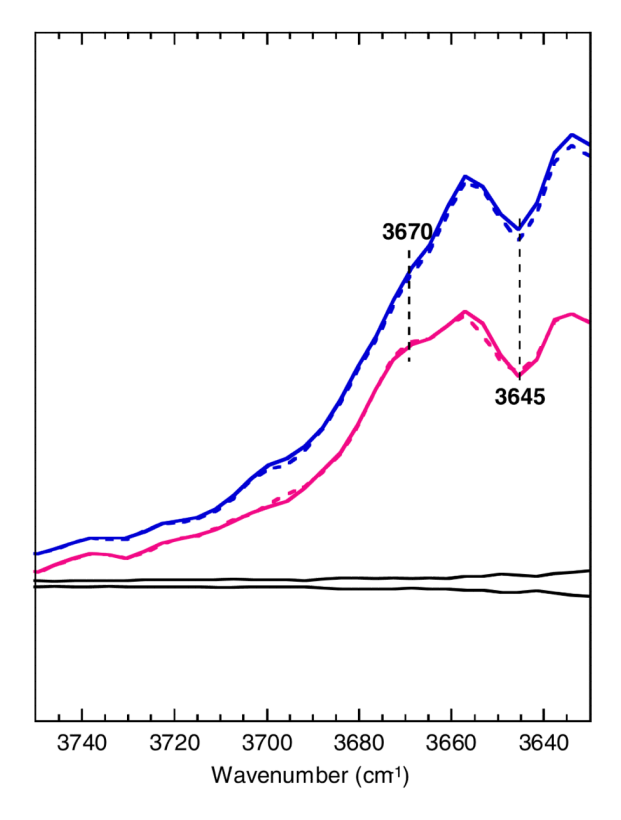
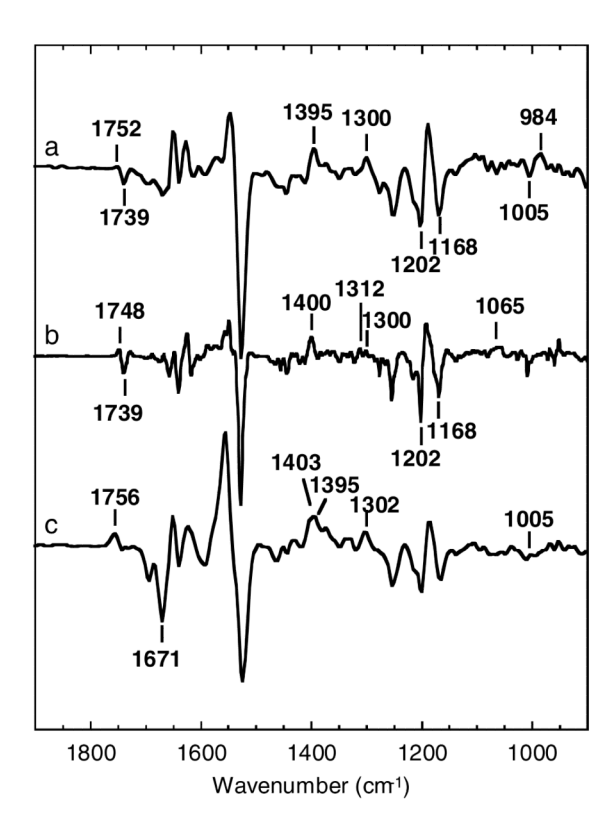


Figure 3. Water O–H stretching vibration bands in  $\rm H_2^{16}O$  (solid lines) and in  $\rm H_2^{18}O$  (broken lines) in the model spectra obtained by a six exponential fit. (a)  $\rm b_1$ . (b)  $\rm b_2$ . (c)  $\rm b_3$ . (d)  $\rm b_4$ . (e)  $\rm b_5$ . (f) Absolute value of residuals averaged for the whole time range. (g) The L-minus-BR spectrum upon illumination at 170 K (41). The amplitude of the 170 K spectrum was normalized using the amplitude of the band at 1202 cm $^{-1}$ . The full length of the ordinate corresponds to 0.0045 AU.



**Figure 4.** Water O–H stretching vibration bands in  $H_2^{16}O$  when the fitting of rate constants was applied to the 3750-3630 cm<sup>-1</sup> region (solid lines, Fit C with 5 exponentials) and for the 1800-900 cm<sup>-1</sup> region (broken lines, Fit B with 6 exponentials). Spectra  $b_1$  and  $b_2$  are shown by blue and red, respectively. The absolute value of residuals averaged for the first 250  $\mu$ s (50 data points) are shown by grey lines. The full length of the ordinate corresponds to 0.0015 AU.



**Figure 5.**Vibration bands due to the Schiff base and Asp96 in the L-*minus*-BR spectrum at 298 K (a), the L-*minus*-BR spectrum at 170 K, obtained as described in (27) (b), and the N-*minus*-BR spectrum at 298 K (c). The full length of the ordinate corresponds to 0.022 AU.

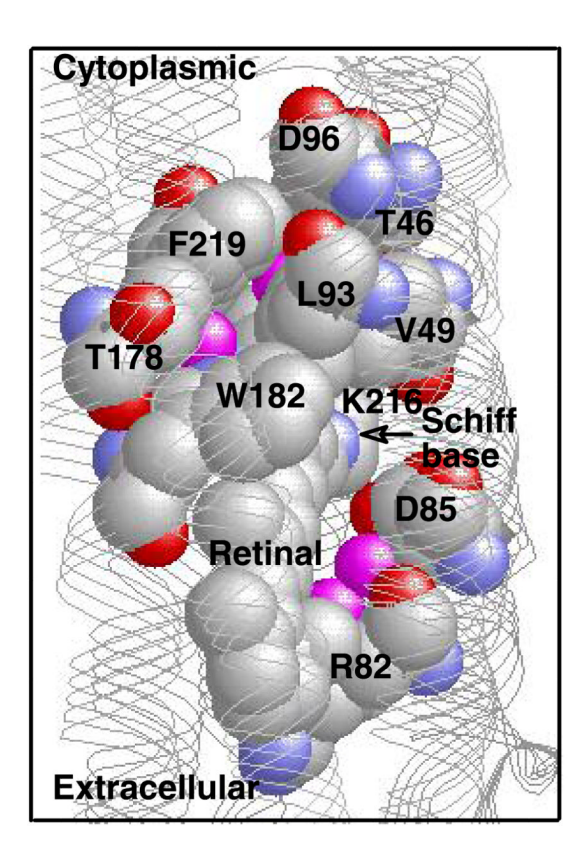


**Figure 6.**Parts of a structural model of the M intermediate of wild-type bacteriorhodopsin showing water molecules surrounded by protein in the region surrounded by Phe219, Asp96, Thr46, Leu93, Trp182, and Thr178, and those interacting with Asp85 and positioned along the sidechain of Arg82. The picture is based on the crystallographic model of Takeda et al. (23); protein data bank entry 1iw9 and was drawn using RasMol.